

On the effect of HPT processing conditions on relative density, mechanical properties and microstructural evolution of hot compacted AA6061– mathematical empirical and response surface approach

Waleed H. El-Garaihy^{1,2*}, Ayman M. Alaskari³, Eisa A. Ameshaiei³, Samy E. Oraby³

¹Mechanical Engineering Department, Unizah College of Engineering, Qassim University, King Abdulaziz St., 51911, Kingdom of Saudi Arabia

²Mechanical Engineering Department, Faculty of Engineering, Suez Canal University, El Salam district, Ismailia 41522, Egypt

³Department of Manufacturing Engineering Technology, College of Technological Studies, P.O. Box 42325, Shuwaikh 76504, Kuwait

*Corresponding author. Tel: (+966) 551108490; E-mail: W.Nasr@qu.edu.sa

Received: 16 September 2016, Revised: 23 October 2016 and Accepted: 03 November 2016

DOI: 10.5185/amlett.2017.1402

www.vbripress.com/aml

Abstract

A loading combination of hot compaction (HC) together with high-pressure torsion (HPT) was used to consolidate discs of AA6061 considering rotations up to 4 revolutions and loading pressure values of 1 and 3 GPa. Mathematical models were established to grasp the true functional interrelationships and variations in the resulting relative densities, mechanical properties, and micro-structural evolutions as affected by the HPT processing pressure and the imposed strain. Sequential iterative nonlinear regression procedures were employed to get the most suitable mathematical relationships that express the relationship between the variables under study. The developed models were examined for its adequacy and significance by using ANOVA analysis as well as many other statistical criteria. Response surface and contour graphs were established for a better understanding of the true functional dependence and, for a quantitative assessment of the intended relationships. It was observed that uniformity of hardness distribution increased with increasing each of the equivalent strain (ϵ_{ef}) and the imposed pressure. A remarkable increase in the compressive strength of deformed discs has been observed. HPT processing produced a tri-model structure with micron scale grains and subgrains, and nano-scale substructure. Copyright © 2017 VBRI Press.

Keywords: AA6061, high pressure torsion, ultrafine grained materials, nonlinear regression procedures, response surface methodology.

Introduction

As a new and promising top-down approach for enhancing the properties of pure metals, processing via severe plastic deformation (SPD) has eventually produced alloys and composites with ultrafine-grained (UFG) and nanocrystalline materials with superior physical, mechanical and multi-functional characteristics [1]. Due to the sample unchanging geometry and shape, the SPD processing technique offers an attractive option because the straining pressure is practically unlimited [2]. Among various available SPD processing methods, two techniques were originated to produce porosity and impurity-free ultrafine-grained bulk crystalline samples with high strength and relatively good ductility [3]. The

most attention has focused on the equal-channel angular pressing (ECAP) and on the high-pressure torsion (HPT) [4, 5]. Recent reviews [6, 7] demonstrated that HPT might be more effective in processing metallic materials to produce exceptionally small grain than ECAP. Accordingly, HPT may have the ability to adjust cumulative strain, applied pressure and strain rate and, at the same time, to obtain UFG materials with a fairly uniform structure if discs are deformed to saturation [8].

HPT has been also utilized for a wide variety of alternative applications such as, grain refinement [9], partial consolidation of hard and brittle materials such as ceramic materials [10] and machining chips [11], the formation and nano-crystallization of amorphous alloys, decomposition of heavily supersaturated solid solutions,

the stabilization of high pressure phases at room temperature and ambient pressure, dissolution of equilibrium phases and, consolidation of metallic composite powders [12, 13].

During HPT processing, a disc is usually placed between two massive anvils. A torsional strain is imposed on the disc by applying a very high pressure to the upper anvil and simultaneously rotating the lower one. During the HPT processing, the specimen expanded outwards into a barrel-shaped configuration to fill the die. Some experimental results are now available where HPT was conducted using larger cylindrical discs [14-16].

Greater strain is then introduced and grain refinement to the submicrometer and/or nanometer range is achieved by the HPT processing as higher strain and strain gradient is developed [17, 18]. The imposed strain varies across the radius of the disc, where the shear strain under HPT can be estimated by the relation [19]:

$$\gamma = (2\pi Nr/h) \quad (1)$$

where, (N) is the number of revolutions, (r) is the distance from the disc center point, and (h) is the deformed disc wall thickness. The corresponding equivalent strain can be calculated from the equation [19]:

$$\varepsilon_{eq} = \ln(2\pi Nr/h) + \ln(h_0/h), \quad (2)$$

where, (h_0) is the initial wall thickness of the disc. The above relation implies that the imposed strain during HPT processing is inhomogeneous across the disc diameter; from a maximum at the edge of the disk to zero in the center where ($r = 0$) [7]. Therefore, a radial dependence of microstructure on the properties of the deformed discs is foreseeable [19]. Despite the implications of inhomogeneity through Eq. (1), and after processing via a relatively small number of revolutions, it showed that there is a gradual evolution in disc's structure, as recorded through hardness results, towards a reasonable level of homogeneity throughout the deformed discs. This level of homogeneity occurred with either increasing of applied pressure, P and/or increasing numbers processing revolutions [7, 18, 20].

The fundamental aim of powder processing techniques is to transform powder into useful bulk component, the conventional powder processing techniques are always accompanied by grain coarsening associated with the sintering process, which results in reducing the mechanical properties. Accordingly, a combination of powder processing and SPD was proposed in the current research to enhance the mechanical properties of the final product through retention and refinement of the consolidated ultrafine powders. In the second hand, an important disadvantage of the HPT is that the processed samples are extremely small [18]. Accordingly, the current study aims to explore the potential for scaling-up the HPT process for use with large samples.

In the current study, the experimental data [21] were utilized to establish a qualitative and quantitative

evaluation approach to explore the effect of the HPT processing conditions on each of the relative density, the mechanical properties, and the microstructural observations of AA6061. Also, the development of a general functional interrelationship describing the dependence of the relative density and hardness of the AA6061 on HPT processing pressure and the number of revolutions applied to the discs were searched for. Response surface in terms of three dimensions and contours graphs were accordingly developed to enhance understanding of the functional dependence of the intended variables so as to be considered as a database reference indicators in the design stages.

Experimental

Micron-powders of AA6061 with an average size of 30 μm were employed as the matrix. Powders were subjected to single sided uniaxial HC into a cylindrical disc of 10 mm in diameter and 9.7 mm in height. The HC process was carried out to produce a partial consolidation of the mixed powders under 525 MPa pressure at a temperature of 673 K (400 °C) over the duration of 30 min.

The HC discs were subjected to HPT as a secondary consolidation processing step. Each die was machined to have a central depression of 4.4 mm deepness and 10 mm in diameter, located centrally on its surface. Torsional straining was achieved by rotation of the lower anvil at a constant speed of 1 rpm. No lubricants were applied on the disc; however, some were applied on the die section adjacent to it. The upper surface of each disc was marked immediately after HPT prior to any microstructural analysis and hardness measurements. HPT was conducted under pressure values of $P = 1$ and 3 GPa, using continuous rotation in a forward direction via 1-up to- 4 revolutions.

The density of the specimens was measured before and after HPT processing using a Mettler Toledo XS 205 digital densitometer that employs the Archimedeian principle for density measurements. Vicker's hardness was tested along the disc cross-section; at center, at half radius, and at the periphery of the HPT-processed discs. Using materials testing system (MTS) the HCs discs were subjected to compression test before and after HPT processing at a value of 500 KN. Furthermore, the discs were compressed at a strain rate of $1 \times 10^{-5} \text{ S}^{-1}$ at room temperature. The micro-structural evolution and consolidation behavior of the discs before and after HPT were characterized by a LEO field emission scanning electron microscopy (FESEM). Average grain intercept (AGI) method was used to determine the average grain and subgrain size. After mounting the AA6061 discs, surface was ground, polished using alumina solution, and finally etched using "keller" instrument.

Data processing modeling methodology

In order to obtain empirical functional interrelationship between a dependent variable, response (Y), and some dependent variables (ξ 's), a first-order general multiplicative model may be proposed [22, 23]:

$$Y = b_0 + \sum_{j=1}^p b_j \xi_j + \varepsilon_n, \quad (3)$$

or in the natural model:

$$Y = b_0 + b_1(x_1) + b_2(x_2) + \dots + b_n(x_n), \quad (4)$$

Regression procedures, based on least squares of errors, were usually employed to estimate the b 's coefficients using the experimental data available.

For possible interaction and quadratic effect among the independent variables (x_i), a second order structure is usually proposed [23]. For instance, considering two independent variables x_1 and x_2 , it takes the form:

$$Y = b_0 + b_1(x_1) + b_2(x_2) + b_{11}(x_1^2) + b_{22}(x_2^2) + b_{11}(x_1x_2), \quad (5)$$

However, whenever data shows a nonlinear pattern, a model of the form (6) is usually proposed [23, 24]:

$$Y = a_0 x_1^{a_1} x_2^{a_2} \dots x_n^{a_n} \quad (6)$$

Regression statistical routine in SPSS-IBM program was used together with the experimental data to obtain the most adequate and significant relationship employing some pre-specified statistical criteria [24, 25].

Within the current analysis, the dependent variables were the relative density (RD), the mechanical properties [Vicker's hardness (Hv), the yield strength (σ_y), the compressive strength (CS), and the fraction strain (ε_f)], in addition to the micro-structural evolution [the grains size (GS) and the subgrains size (SGS)]. The considered independent variables were the HPT processing pressure (P) and the number of revolutions (N).

Progressive strategy is followed starting with a first-order model of form (3). If such a model prevailed, through residuals examination, a tendency to variables interaction and/or quadratic, a promoted model of form (5) should be suggested instead. Furthermore, whenever nonlinearity attitude is detected, a sophisticated nonlinear structure in form (6) is recommended. Fitting procedures were terminated once the best model is detected. Model adequacy and significant were judged through many ANOVA parameters and criteria using correlation factor (factor of determination) R^2 , $t_{\text{statistics}}$ value and F_{ratio} [23, 24].

While correlation factor R^2 usually measures the percentage of variation in the response variable (Y) explained by the explanatory variable x, the student $t_{\text{statistics}}$ value usually measures the influence strength (weight) of an estimated coefficient for a specific independent variable x_i through comparing its estimated value to its calculated standard error. However, F_{ratio} (F-test) usually judges the ratio of regression mean squares to the residuals mean squares for a set of independent variables and number of data points (degrees of freedom).

Based on the final accepted significant and adequate models, a response surface was developed using Surfer program.

It is important to affirm here that the developed models are of empirical nature that is valid only for the data domain for which they were established. Generally, regression models can be interpolated but a possible trend extrapolation always requires further data extension.

Results and discussion

Effect of HPT processing conditions on the relative density

The aforementioned fitting strategy is used to establish a relationship between the relative density (RD) of the AA6061 discs, as a dependent variable, and both of the HPT processing revolutions (N) and pressure (P) as independent variables using the experimental data listed in (Table 1) (See the supplementary information file). The nonconventional nonlinear iterative regression routine in SPSS program was used according to the default convergence criteria. The model derivatives are numerically calculated and examined against the specified criterion values. The process continues until it reaches the best model with minimum squares of residuals relevant to the specified criteria. This process has led to the model (7).

$$RD\% = 98.6(N + 1)^{0.006} \quad (7)$$

with R^2 of 90.6% along with $t_{\text{statistics}}$ of 1280, and 6 together with F_{ratio} value of 2763937. Such excellent values confirmed the significance and adequacy of the developed model. Technical interpretations of the developed model indicate that while the pressure (P) is found insignificant to enter the relation, the number of revolutions (N) is found to have a slight effect of the relative density (RD %).

To examine the goodness of the resulting equation, predicted (estimated) values are compared to the experimental counterparts as shown in Fig. 1 (in the supplementary information file). Fig. 1a is dedicated to indicating how predicted values are close to its counterparts the experimental ones (Table 1 as shown in the supplementary information file). The residuals distribution for the HPT-processed discs RD% is shown in Fig. 1b. The effect of the number of revolutions and the imposed pressure on RD% for AA6061 compared to the predicted values from the model (7) is shown in Fig. 1.

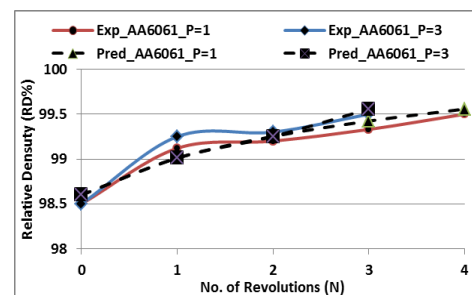


Fig. 1. The effect of HPT processing pressure and number of revolutions on RD of AA6061 disc compared to the predicted RD-values from model (7).

From **Fig. I** and **Fig. 1** it can be seen that the nonlinear model (7) produces accurate estimation values regarding RD%-N interrelationship. The developed nonlinear model (7) showed quick rapid iterative convergence with tight confidence intervals (low residuals range). Also, examination of the residuals revealed nothing against their normality (no observed pattern). From the experimental results (**Table 1**) together with **Fig. I** and **Fig. 1**, some obvious and important trends for materials processed by HPT have been emerged. All plain AA6061 discs processed via HPT revealed higher relative density (RD %) compared to the hot compacted counterparts (The relative density produced for the as-HC condition was 98.5). Increasing the imposed strain through increasing the number of revolutions resulted has led to an increase the RD of the AA6061 discs. This can be stated that increasing the relative density (RD %) of the Al-alloy discs after HPT processing can be explained by the huge shear deformation applied. Accordingly, the shear deformation can facilitate the reduction of porosity; it can assist all three porosity reduction mechanisms (movement of particles into voids, deformation of particles, and flattening of the microscopic and submicroscopic features on the particle surface) [25] which can be attributed to the role of shear strain on the consolidation process based on particles localized fragmentation, mechanical interlocking, and realignment of the particles. In addition, the high imposed shear strain which accompanied HPT processing resulted in significant grain refinement which increases grain-to-grain contact surface that resulted in reducing porosity and hence increasing the relative density of the HPT-processed discs. In addition, the shear deformation may result in breaking-down the oxide layers which are naturally formed on the surface of Al-powder particles. These layers are known to significantly hinder effective bonding during sintering of Al-powder particles [26]. Breaking off this barrier can improve the cold and warm welding strength and sintering response by exposing oxide free surface which enhances diffusion [26].

Effect of HPT processing conditions on the hardness

The same fitting procedure and strategy, which has been explained in the last section, are followed to develop a functional interrelationship between the alloy Hv-values as a dependent variable and both of the HPT processing revolutions (N), the position from the disc center (R) [at the center of the disc (R_0), at midway between the disc center and its periphery ($R_{0.5}$), at the periphery (R_1)], and processing pressure (P) as influential independent variables.

The non-linear model is found to have the following structures:

$$Hv = 65.95(N + 1)^{(0.353)}(R + 1)^{(0.256)}, \quad (8)$$

with R^2 of 83.6% along with $t_{\text{statistics}}$ of 18.3, 93 and, 3.7 together with F_{ratio} value of 915. Accordingly, model (8) is with good statistical criteria that satisfy the adequacy requirements. **Fig. IIa** (as shown in the supplementary

information file) is dedicated to indicating how predicted (estimated) values are close to its counterpart experimental values. In addition, the residuals distribution for the Hv-values is shown in **Fig. IIb**. However, residuals indicate a convergence pattern as a function of the test order. This does not imply time-dependence experimental error due to inaccuracy in the testing hardware or in measuring instruments. Experiments were carried out in a random sequence. Again, a model (8) indicates that the imposed pressure (P) was not significant enough to enter the equation an influential parameter.

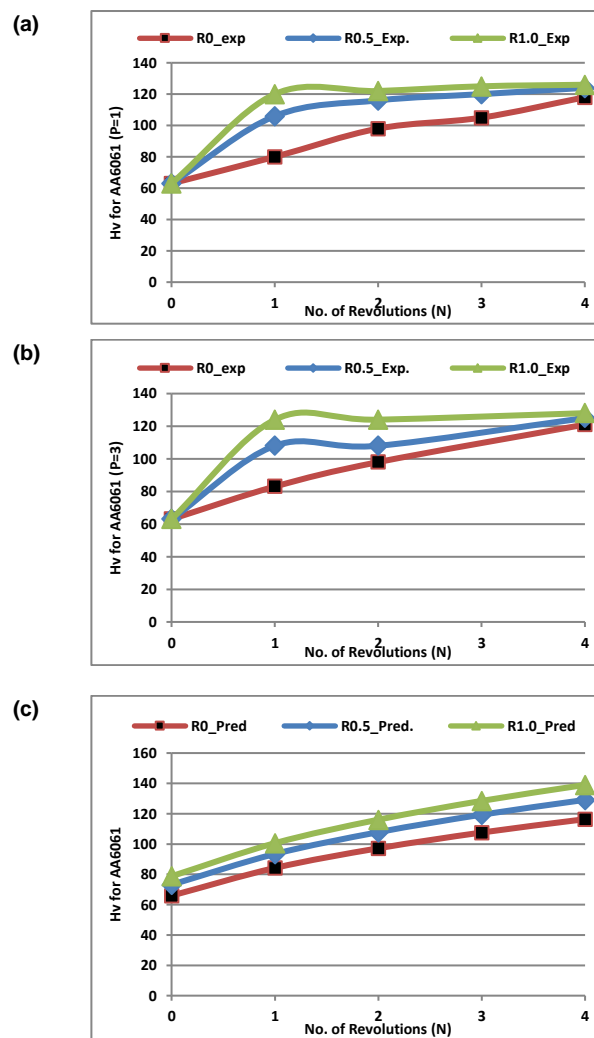


Fig. 2. The effect of number of revolutions (N) on Hv-values of AA6061 disc processed at a pressure of (a) 1 GPa , (b) 3 GPa compared to (c) predicted Hv-values from model (8).

From model (8) it is clear that the HPT processing pressure was not effective enough to impose its possible effect on Hv-values. Experimental effects of the number of revolutions and the position from the disc center on Hv-values at different processing pressures for AA6061 compared to the predicted values from model (8) are shown in **Fig. 2**.

From **Fig. 2** it is revealed that the predicted (estimated) values are close to its counterpart experimental values for the AA6061 discs processed at a pressure of 1 and 3 GPa. It is clear that the lower hardness values were reported at

the centers of discs while the higher values are detected at the peripheral regions.

It is reasonable to conclude from these results that the increase in the Hv-values with increasing applied pressure was due to the development of higher Hv-values around the peripheries of the discs and, subsequently, a homogeneous distribution of high hardness zone swept across the discs. Recent experiments showed that the applied high pressure led to a significant increase in hardness across the discs cross-section even in the absence of any torsional straining [17].

In addition, **Fig. 2** showed that the Hv-values of the AA6061 discs processed at 1 GPa at a different number of revolutions were very close to the counterparts processed at 3 GPa. The insignificant increase in the Hv-values noticed in the discs processed at 3 GPa compared to the counterparts processed at 1 GPa can be attributed to the relatively unimportant slippage in Al alloys below applied pressure of 3 GPa.

Fig. 3 indicates response surfaces and contours for each of the experimental results and the corresponding predicted values using model (8). The functional Hv-N-R relationships are well qualitatively explained. It is shown a strong influence of both N and R on the deformed product. However, surfaces indicate that Hv nonlinearly increases as each of N and R increases with a higher slope for N.

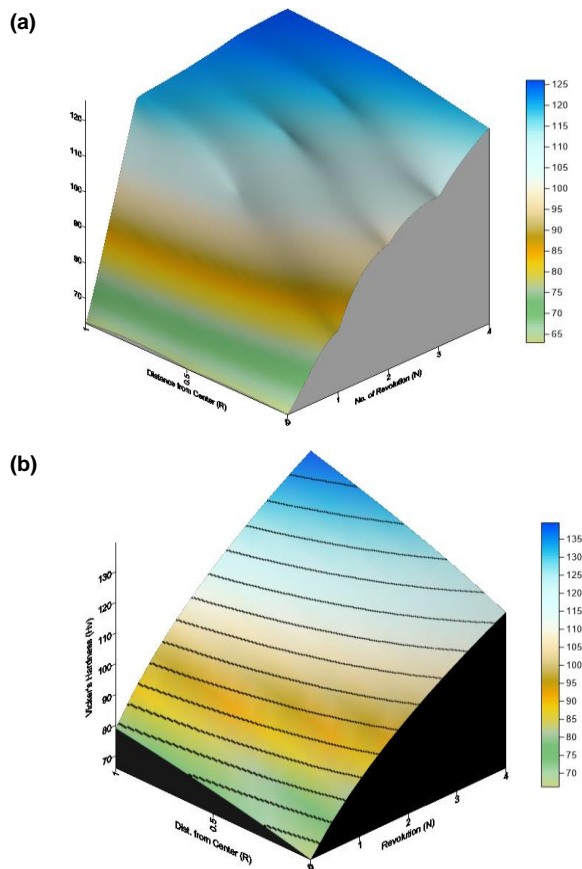


Fig. 3. Response surface and contours for (a) experimental results and (b) corresponding predicted values using model (8) for Hv of AA6061 discs processed via HPT.

A quantitative evaluation of the results is diagrammatically expressed in details within **Fig. 2** and **Fig. III** (as shown in the supplementary information file). It is shown that a 1-revolution has resulted in increasing the Hv-values of AA6061 from 80 at the center of the disc to 122 at the peripheries. This indicates a significant degree of inhomogeneity in the distribution of properties across the cross section of the disc. However, this hardness inhomogeneity gradually disappeared with further straining up to 4-revolutions leaving reasonably constant Hv-distribution over the entire disc with an average value of Hv = 125 which mean that the Hv-values increased by ~ 200% post HPT processing compared to the un-processed counterparts as shown in **Fig. 2** and **Fig. III** which agreed with [14].

The Hv-values along the cross-section area of AA6061 discs processed by HPT in this work were in full agreement with what reported by other authors considering materials with face-centered cubic (FCC) structure and low stacking faults energy (SFE) [27]. Higher hardness values were reported in the peripheral regions and lower values at the center of the discs. Knowing that AA6061 alloy has low SFE, recovery usually occurs at a slower rate, which produces a steady state increase in the rate of hardening through the initial stages of processing [28]. Lower recovery rates usually cause a high initial strain hardening that is associated with friction at the discs-die walls interface compared to lower hardness in the central region [8, 29]. As the torsional strain continued to reach a sufficiently high total value, a homogeneous hardness distribution along the disc cross section was observed. This was consistent with the basic concepts of the strain gradient plasticity modeling that were developed to explain the evolution of homogeneity with increasing numbers of revolutions when processing in HPT [8].

In order to obtain a more clear interpretation of the effect of rotation on the hardness, a relationship between hardness variations ($Hv_{\text{variation}} = Hv_{N=0} - Hv_{N=1,2,3,4}$) and both the influential parameters (N) and (R) was established to have the form:

$$Hv = 32.911 N^{(0.244)} (R + 1)^{(0.625)}, \quad (9)$$

with $R^2 = 75$; $t_{\text{statistics}} = 12, 4, 5.3$; and $F_{\text{ratio}} = 345$, the developed model (9) is found reasonable enough to represent the experimental data.

Fig. 4 indicates the hardness variation attitudes as it has been affected by (N) and (R) using both the experimental data, **Fig. 4a**, and those extracted from model (9), **Fig. 4b**. As can be seen from response surface topography and contour maps, a very accurate quantitative and qualitative correlation is obtained. Vicker's hardness is prominently influenced by each of (N) and (R) especially at $N \geq 3$ and $R \geq 0.5$.

The strengthening mechanisms associated with SPD may include solid solution strengthening, strain hardening, grain refinement strengthening, as well as oxide dispersion strengthening [29-31].

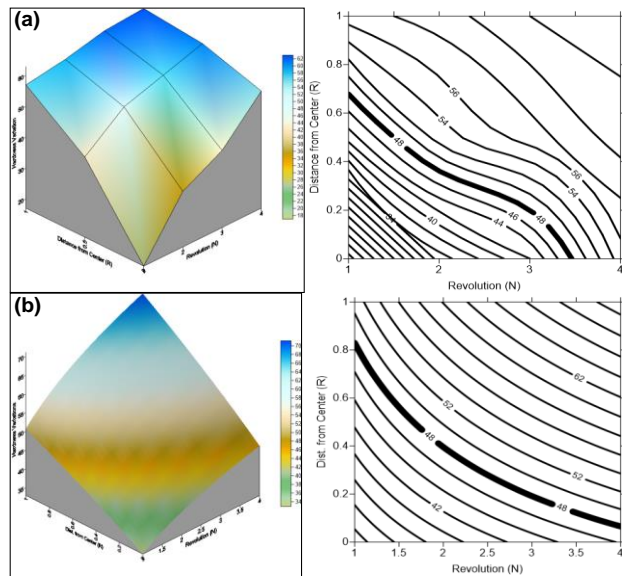


Fig. 4. Hardness variations as affected by (R) and (N).

The interstitial and substitution solute atoms of the alloying elements in AA6061 distort the crystal lattice, resist dislocation mobility, and hence strengthen the alloy. Dislocation piling at the boundaries resulted in increasing resistance to deformation and hence higher hardness.

Dislocation strengthening assisted significantly in the strength and hardness enhancement. The excess dislocations within grains and subgrain boundaries make dislocation glide more difficult. The dislocation density usually increases with HPT processing, due to dislocation multiplication or the formation of new dislocations. Thus the mobility of a dislocation is reduced by the presence of other dislocations, which is consistent with the significant increase of hardness after HPT processing [28, 30, 32].

Effect of HPT processing conditions on the compressive properties

Similar fitting procedures and strategy were followed to develop a functional interrelationship between the AA6061 yield stress (σ_y), the compressive strength (CS), and the fracture strain (FS), as dependent variables and both of the HPT processing revolutions (N), and the processing pressure (P) as influential independent variables.

The non-linear model has been found to have the following structures for the yield strength {model (10)}, the compressive strength {model (11)}, and the fracture strain {model (12)}, respectively:

$$\sigma_y = 225.2 (N + 1)^{(0.179)}, \quad (10)$$

with R^2 of 85% along with $t_{\text{statistics}}$ of 29.5 and, 6.2 together with F_{ratio} value of 1950.

$$CS = 249.15 (N + 1)^{(0.171)}, \quad (11)$$

with R^2 of 85% along with $t_{\text{statistics}}$ of 31 and, 6.1 together with F_{ratio} value of 2134.

$$S = 29.023 (N + 1)^{(-0.948)}, \quad (12)$$

with R^2 of 93% along with $t_{\text{statistics}}$ of 16.2 and, -8.7 together with F_{ratio} value of 128.

Accordingly, it is clear that the developed models (10-to-12) are considered adequate and significant to represent the relevant functional interrelationship.

Once more, the imposed pressure (P) was not significant enough to enter the equation as an influential parameter on any of the yield strength, the compressive strength or the fracture strain.

For practical predictability comparison between the experimental and the predicted results of the nonlinear models, Fig. 5 is dedicated to indicate how predicted (estimated) value is close to its counterpart experimental value for both the yield stress (Fig. 5a), the compressive strength (Fig. 5b), and the fracture strain (Fig. 5c). From the models (10- to -12) it is clear that the HPT processing pressure has insignificant influence on the compressive properties, especially on the fracture strain.

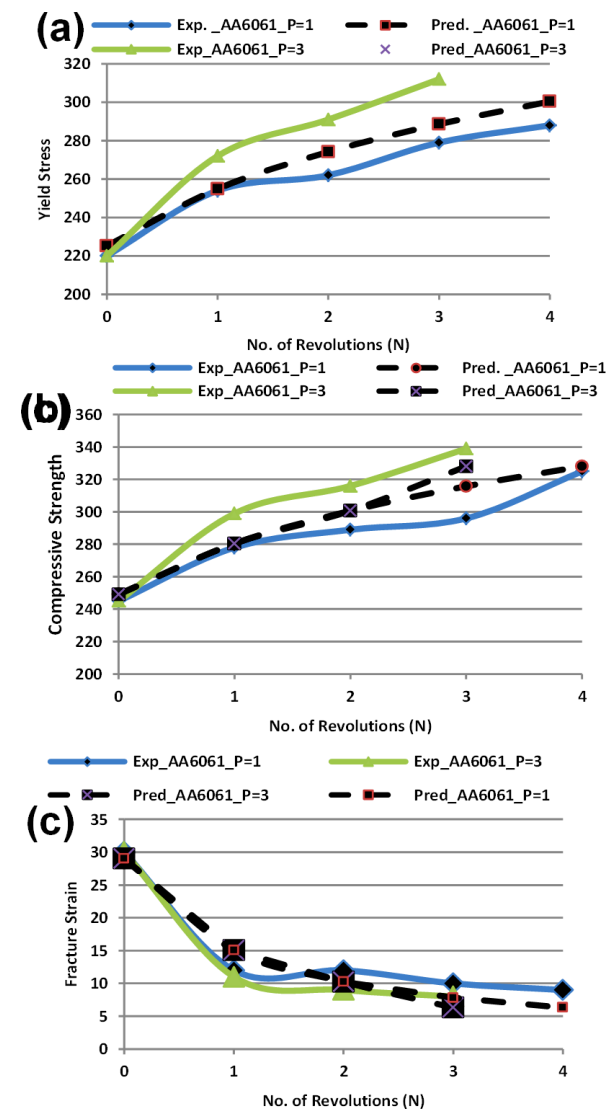


Fig. 5. Experimental results vs. predicted ones of (a) yield stress, (b) compressive strength, and (c) fracture strain of AA6061 processed via HPT.

It can be revealed that, the compressive strength and the yield strength of deformed AA6061 discs were significantly higher than that of their un-deformed counterparts. At the same time, compressive strength and the yield strength of the HPT-processed discs increased significantly with increasing the imposed strain, which was accompanied with a decrease in the ductility.

A significant increase of the material strength after HPT processing can be mainly attributed to the formation of the homogeneous UFG microstructure that provided a significant strengthening according to the Hall-Petch law [33]. From this relationship, it is readily apparent that the materials strength post HPT should be increased because of their extremely small grain sizes. Based on Hall-Petch relationship, the refinement of the material's structure to nano-scale level has led to an increase in its strength.

In addition, finer grains size usually increases the grain boundaries area that impedes dislocation motion. These pile-ups introduce stress concentrations ahead of their slip planes, which generate new dislocations in adjacent grains [34].

Effect of HPT processing conditions on the microstructural evolution

SEM analysis was employed in order to investigate the internal structure of AA6061 HCs discs before and after HPT processing. The microstructure of the as-HC discs of AA6061 is shown in **Fig. IV** (as shown in supplementary information file). **Fig. 6** shows microstructural evolution of the discs surfaces at the peripheries post HPT processing via 1-rev. (a, c), and 4-rev. (b, d) at a pressure of 1 GPa (a, b) and 3 GPa (c, d), respectively.

The SEM micrographs confirmed the potential for achieving UFG after HPT processing. Influence of the amount of strain via increasing the number of revolutions from 1-up to 4 revolutions on the size and shape of the grains, the subgrains, and the substructure developed during deformation was clearly depicted at the displayed micrographs. The average grains, subgrains, and substructure sizes of 35, 3.2 μm , and 610 nm, respectively. HPT straining via $\epsilon_{\text{eq}} = 1.57$ (corresponding to $N = 1$ -rev.) resulted in refining the grains, subgrains, and substructure sizes to 33, 2.8 μm , and 360 nm, respectively. Increasing the amount of strain up to $\epsilon_{\text{eq}} = 3.1$ (4-rev.) revealed further refinement of the grains, subgrains, and substructure sizes to 30, 1.9 μm , and 250 nm (**Fig. 6a, b**).

Increasing the HPT processing pressure from 1 up to 3 GPa resulted in an additional slight refinement of the grains, subgrains and substructures. Due to the SPD induced with increasing number of revolutions up to under pressure of 3 GPa, the consolidated powders equiaxed subgrains were elongated but rather in different directions following the orientation of slip planes as shown in **Fig. 6d**.

The fitting procedures have led to the following nonlinear functional interrelationship between the alloy grain, subgrain, and substructure size (GS, SGS, and SSS, respectively) as a dependent variable and both of the HPT

processing revolutions (N) and processing pressure (P) as influential independent variables.

$$GS = 34.86(N + 1)^{(-0.1)}, \quad (13)$$

with R^2 of 78.5 % along with $t_{\text{statistics}}=126$ and, -12.5 together with F_{ratio} value of 358, the developed model is considered adequate and significant to represent the relevant functional interrelationship.

$$SGS = 3.157(N + 1)^{(-0.321)}, \quad (14)$$

with R^2 of 96% along with $t_{\text{statistics}} = 17.6$ and, -5.2 together with F_{ratio} value of 23895, the model satisfies the adequacy requirements.

$$SSS = 587.24 (N + 1)^{(-0.614)}, \quad (15)$$

with R^2 of 89.4 % along with $t_{\text{statistics}} = 17$ and, -7.8 together with F_{ratio} value of 254, therefore, it is concluded that it is adequate and significant enough to represent the set of experimental data for which it was developed.

Fig. V (supplementary information file) shows a comparison between the experimental and the counterpart predicted results. Also, residual values and distribution for each parameter are included. The influence of the HPT processing pressure and a number of revolutions on microstructural evolutions for AA6061 compared to the predicted values from models (13-to-15) is shown in **Fig. 7**.

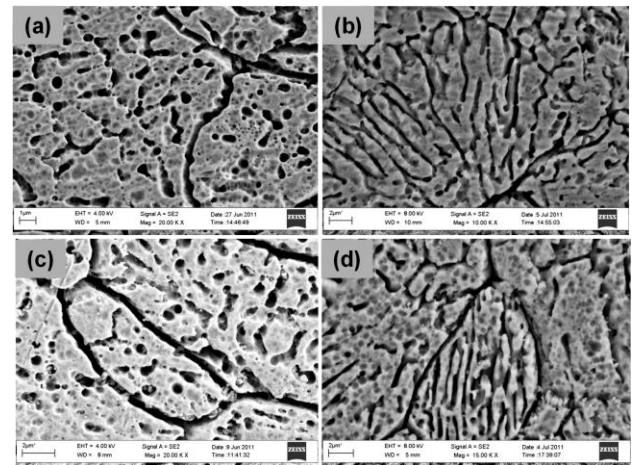


Fig. 6. SEM micrographs of AA6061 discs processed at 1 GPa (a, b) and 3 GPa (c, d) via (a, c) 1-revolution, and (b, d) 4-revolutions, respectively.

As shown in **Fig. 6**, intensity of deformation was observed via the alignment of the AA6061 consolidated grains in the direction of shear, which increased with increasing the number of revolutions and/or the imposed pressure. Due to the SPD induced with increasing amount of strain, the consolidated powders equiaxed subgrains were elongated but rather in different directions following the orientation of slip planes as shown in **Fig. 6d**. Even within the same grain, several orientations of the

subgrains showed deformation on more than one slip system indicative of multiple slips. The different orientation of the grains made it more difficult for the dislocation to change its direction of motion which resulted in increasing the hardness and the strength of the processed disc.

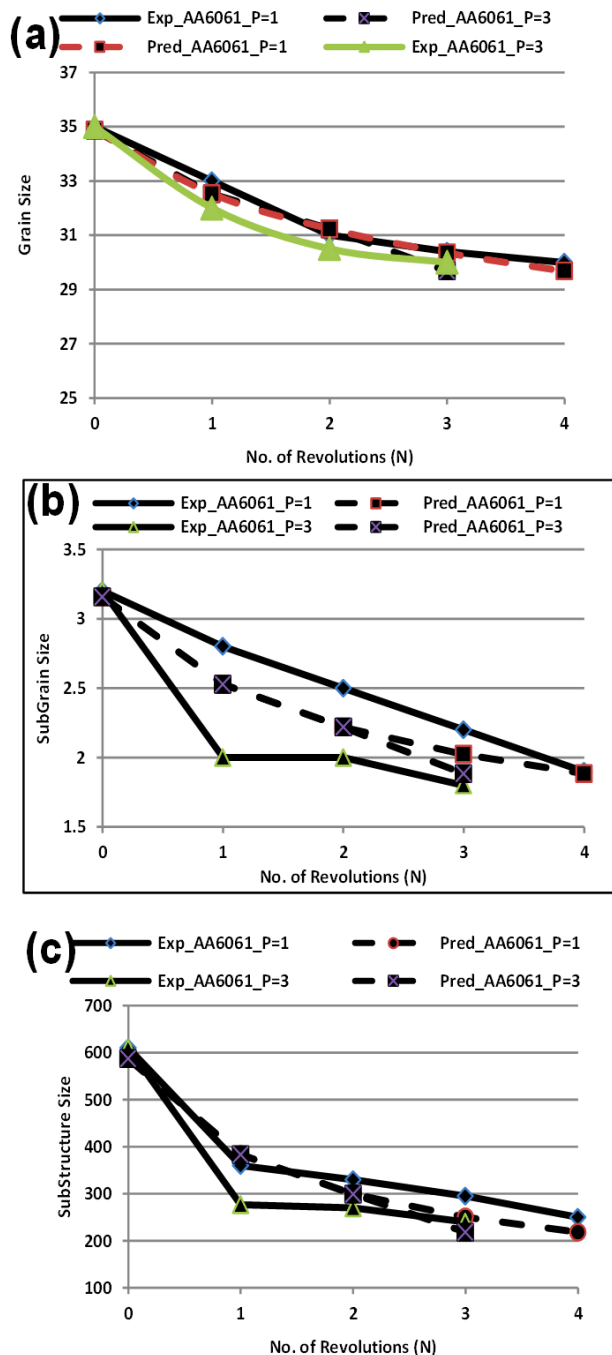


Fig. 7. The effect of HPT processing pressure and number of revolutions on (a) grains, (b) subgrains, and (c) substructure size of AA6061 disc compared to the predicted values from models (13-to-15).

This could provide an indication of the evolution of substructure of medium-to-high angle boundaries. Further investigation with TEM is necessary to validate this observation. This agreed with the fact that in the (FCC) metals the grains were refined by the formation of arrays

of subgrains and subsequent evolution of low-angle boundaries into boundaries having high angles of misorientation [14].

A combination of strain hardening and dynamic recovery might have resulted in the observed slight increase in grains and subgrains refinement associated with the increased misorientation on the subgrain level as the imposed pressure increased from 1 GPa (**Fig. 6a, b**)-to-3 GPa (**Fig. 6c, d**). This in-turn influenced positively the hardness level measured post HPT processing. Since dislocations were introduced into the discs throughout HPT processing, it can be concluded that saturation corresponded to a condition where the rate of dislocation nucleation was approximately balanced by the rate of recovery [35].

Conclusion

Discs of AA6061 successfully produced via a combination of HC followed by HPT processing to nearly 99.5 % of the theoretical density. HPT processing was conducted under different conditions of pressures and numbers of revolutions at room temperature. Nonlinear model structures are proposed with sequential preference strategy and robust statistical criterion judgment to examine the model predictability and its residuals pattern. For the set of experimental data investigated, all the developed models are found significant and adequate to act as a good prediction tool only for the data domain under investigation. A universal model can be then reached whenever the experimental domain is widened. It was found that the developed models indicated that the imposed pressure (P) was not significant enough to enter the equation an influential parameter. It was clear that HPT processing has improved densification of HC discs. In addition, Hv-values of the HC discs increased by 200% post HPT processing for AA6061 consolidated powders. It was clear that the uniformity of hardness distribution throughout the discs increased with increasing the equivalent strain. HPT processing produced trimodal structure with micro-scale grains and subgrains, and nano-scale substructure. For AA6061 discs processed via HPT produced significant grain refinement an average grain, subgrain and substructure sizes of 28, 1.8 μm , and 240 nm, respectively. Accordingly, increasing the imposed pressure to 3GPa resulted in a slight increase in the intensity of deformation of the consolidated discs.

Acknowledgements

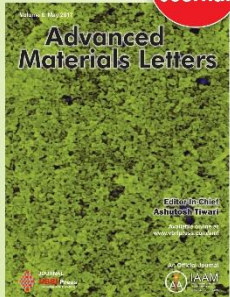
The authors are grateful to Youssef Jamil Science and Technology Research Center (YJSTRC) and the Mechanical Engineering Department of The American University in Cairo-Egypt for financial support and continuous assistance of their lab engineers and research assistances.

Author's contributions

Performed the experiments: W.H.G.; Data analysis: W.H.G., E.A.A., A.E.A., S.E.O.; Wrote the paper: W.H.G., S.E.O.; Reviewing and modifying the discussion: E.A.A. Authors have no competing financial interests.

References

- B. Oberdorfer, B.; Setman, D.; Steyskal, E.; Hohenwarter, A.; Sprengel, W.; Zehetbauer, M.; Pippin, R.; Wurschum, R; *Acta Mater.*, **2014**, 68, 189.
DOI: [S1359645413009816](https://doi.org/10.1016/j.actamat.2014.04.008)
- Zhilyaev, A.P.; Sergeev, S.N.; Langdon, T.G.; *Jmr&t*, **2014**, 3, 338.
DOI: [S2238785414000556](https://doi.org/10.1016/S0921-5093(99)00764-9)
- Patil, D.C.; Das, M.; Das, G.; Kori, S.A.; Venkateswarlu, K.; *Procedia Materials Science*, **2014**, 5, 379.
DOI: [S2211812814006452](https://doi.org/10.1016/S2211812814006452)
- A. Y. Khereddine, Larbi, F.H.; Kawasaki, M.; Baudin, T.; Bradai, D.; Langdon, T.G.; *Mater. Sci. Eng. A*, **2013**, 576, 149.
DOI: [S0921509313003717](https://doi.org/10.1016/S0921509313003717)
- Revesz, A.; Kis-Toth, A.; Varga, L.K.; Schafler, E.; Bakonyi, I.; Spassov, T.; *Int. J. Hydrogen Energ.*, **2012**, 37, 5769.
DOI: [S0360319911028941](https://doi.org/10.1016/j.ijhydeng.2012.08.041)
- Draï, A.; Aour, B.; *Eng. Struct.*, **2013**, 46, 87.
DOI: [S0141029612003422](https://doi.org/10.1016/j.engstruct.2013.04.022)
- Kawasaki, M.; Foissey, M.J.; Langdon, T.G.; *Mater. Sci. Eng. A*, **2013**, 561, 118.
DOI: [S0921509312015316](https://doi.org/10.1016/S0921509312015316)
- Estrin, Y.; Molotnikov, A.; Davies, C.H.; Lapovok, R.; *J. Mech. and Phys. Solids*, **2008**, 56, 1186.
DOI: [S0022509607002001](https://doi.org/10.1016/j.jmps.2008.06.001)
- Liu, M.; Rován, H.J.; Liu, X.; Murashkin, M.; Valiev, R.Z.; Ungar, T.; Balogh, L.; *J. Mater. Sci.*, **2010**, 45, 4659.
DOI: [S10853-010-4604-3](https://doi.org/10.1007/s10853-010-4604-3)
- Edalati K.; Horita, Z.; *Scripta Mater.*, **2010**, 63, 174.
DOI: [S1359646210001867](https://doi.org/10.1016/j.scriptamat.2010.08.017)
- Zhilyaev, A.P.; Gimazov, A.A.; Raab, G.I.; Langdon, T.G.; *Mater. Sci. Eng. A*, **2013**, 486, 123.
DOI: [S0921509307016176](https://doi.org/10.1016/S0921509307016176)
- Srinivasarao, B.; Zhilyaev, A.P.; Langdon, T.G.; Perez-Prado, M.T.; *Mater. Sci. Eng. A*, **2013**, 562, 196.
DOI: [S0921509312015754](https://doi.org/10.1016/S0921509312015754)
- Srinivasarao, B.; Zhilyaev, A.P.; Gutierrez-Urrutia, I.; Perez-Prado, M.T.; *Scripta Mater.*, **2013**, 68, 583.
DOI: [S1359646212007816](https://doi.org/10.1016/S1359646212007816)
- Salem, H.G.; El-Garaihy, W.H.; Abdel Rassoul, E.M.; *Materials Processing and Interfaces, TMS Supplemented Proceeding*, **2012**, 1, 553.
DOI: [10.1002/9781118356074](https://doi.org/10.1002/9781118356074)
- Figueiredo, R.B.; Aguilar, M.T.; Cetlin, P.R.; Langdon, T.G.; *Metall. Mater. Trans. A*, **2011**, 42, 3013.
DOI: [S11661-011-0609-z](https://doi.org/10.1007/s11661-011-0609-z)
- Kawasaki, M.; Lee, H.J.; Ahn, B.; Zhilyaev, A.P.; Langdon, T.G.; *Jmr&t*, **2014**, 3, 311.
DOI: [S2238785414000490](https://doi.org/10.1016/S2238785414000490)
- Song, Y.; Yoon, E.Y.; Lee, D. J.; Lee, J. H.; Kim, H.S.; *Mat. Science and Engineering A*, **2011**, 528, 4840.
DOI: [S0921509311001717](https://doi.org/10.1016/S0921509311001717)
- Zhilyaev, A. P.; Langdon, T. G.; *Progress in Materials Science*, **2008**, 53, 893.
DOI: [S007964250800025X](https://doi.org/10.1016/S007964250800025X)
- Ghosh, K.S.; N. Gao, M.J. Starink; *Materials Science and Engineering A*, **2012**, 552, 164.
DOI: [S0921509312007186](https://doi.org/10.1016/S0921509312007186)
- Huang, Y.; Kawasaki, M.; Langdon, T. G.; *J Mater. Sci.*, **2012**, 48, 6517.
DOI: [S10853-012-7015-9](https://doi.org/10.1007/s10853-012-7015-9)
- W.H. El_Garaihy; Ph.D Thesis, Mansoura University, Egypt, **2012**.
DOI: http://www.eulc.edu.eg/eulc_v5/Libraries/Thesis/BrowseThe sisPages.aspx?fn=PublicDrawThesis&BibID=11842944
- Douglas, C.M.; Elizabeth, A.P.; Geoffrey, G.V.; *Introduction to Linear Regression Analysis*; John Wiley & Sons; USA, **2012**.
DOI: <http://eu.wiley.com/WileyCDA/WileyTitle/productCd-0470542810.html>
- Myers, R.H.; Montgomery, D.C.; Vining, G.G.; Robinson, T.J.; *Generalized Linear Models: With Applications in Engineering and the Sciences*; John Wiley & Sons; USA, **2012**.
DOI: <http://eu.wiley.com/WileyCDA/WileyTitle/productCd-0470454636.html>
- Kowalski, B.R.; *Chemometrics: Theory and Application*; 52; ACS Publications, Chemometrics, USA, Theory and Application, **1977**.
DOI: <http://pubs.acs.org/isbn/9780841203792>
- Stolyarov, V.V.; Zhu, Y.T.; Lowe, T.C.; Islamgaliev, R.K.; Valiev, R.Z.; *Materials Science and Engineering, A*, **2000**, 282, 78.
DOI: [10.1016/S0921-5093\(99\)00764-9](https://doi.org/10.1016/S0921-5093(99)00764-9)
- Wei, X.S.; Vekshin, B.; Kraposhin, V.; Huang, Y.J.; Shen, J.; Xia, K.; *Materials Science and Engineering A*, **2011**, 528, 5784.
DOI: [S0921509311003996](https://doi.org/10.1016/S0921509311003996)
- T.G. Langdon, and C. Xu; *Mat. Sci. and Engineering*, **2009**, 71.
DOI: [S0921509308008988](https://doi.org/10.1016/S0921509308008988)
- T.G. Langdon, T.G.; C. Xu, C.; Horita and Z.; *Acta Materialia*, **2008**, 56, 5168.
DOI: [S1359645408004667](https://doi.org/10.1016/S1359645408004667)
- Wetscher, F.; Vorhauer, A.; Pippin, R.; *Material Science and Engineering, A*, **2005**, 410, 213.
DOI: [S0921509305008221](https://doi.org/10.1016/S0921509305008221)
- Zhang, J.; Gao, N.; Starink, M. J.; *Materials Science and Engineering A*, **2010**, 527, 3472.
DOI: [S0921509310001656](https://doi.org/10.1016/S0921509310001656)
- Valiev, R.Z.; Rován, H.J.; Liu, M.; Murashkin, M.; Kilmametov, A.R.; Ungar, T.; Balogh, L.; *Materials Science Forum*, **2009**, 604, 179.
DOI: [MSF.604-605.179](https://doi.org/10.1016/S0921509310001656)
- Edalati, K.; Daio, T.; Horita, Z.; Kishida, K.; Inui, H.; *J. of Alloys and Compounds*, **2013**, 563, 221–228.
DOI: [S0925838813004362](https://doi.org/10.1016/j.jallcom.2013.04.032)
- Loucif, A.; Figueiredo, R.B.; Baudin, T.; Brisset, F.; Chemam, R.; Langdon, T. G.; *Materials Science and Engineering A*, **2012**, 532, 139.
DOI: [S0921509311011762](https://doi.org/10.1016/S0921509311011762)
- Tian, Y.Z.; Wu, S.D.; Zhang, Z.F.; Figueiredo, R.B.; Gao, N.; Langdon, T.G.; *Acta Materialia*, **2011**, 59, 2783.
DOI: [S1359645411000231](https://doi.org/10.1016/S1359645411000231)
- Langdon, T.G.; Sakai, G.; Horita, Z.; *Materials Science and Engineering A*, **2005**, 393, 344.
DOI: [S0921509304013310](https://doi.org/10.1016/S0921509304013310)



Copyright © 2017 VBRI Press AB, Sweden

A Monthly Journal

Publish your article in this journal

Advanced Materials Letters is an official international journal of International Association of Advanced Materials (IAAM, www.iaamonline.org) published monthly by VBRI Press AB from Sweden. The journal is intended to provide high-quality peer-review articles in the fascinating field of materials science and technology particularly in the area of structure, synthesis and processing, characterisation, advanced-state properties and applications of materials. All published articles are indexed in various databases and are available download for free. The manuscript management system is completely electronic and has fast and fair peer-review process. The journal includes review article, research article, notes, letter to editor and short communications.

www.vbripress.com/aml

Supplementary Information

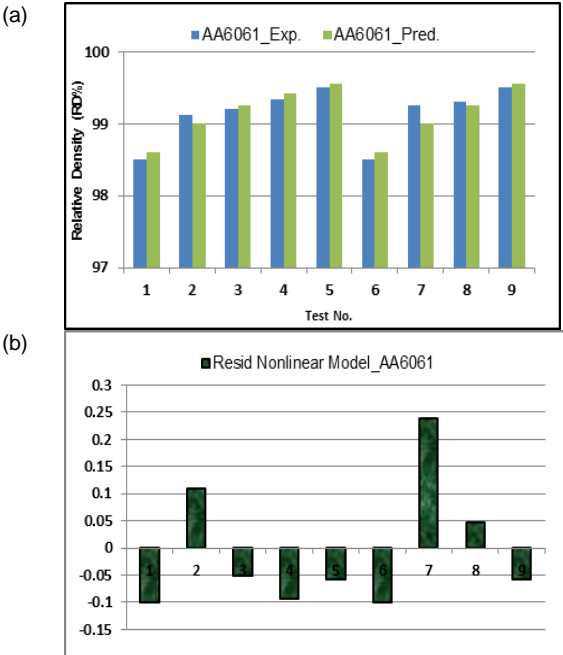


Fig. I. Experimental results vs. predicted (a) and the residuals distribution (b) of the RD for the HPT-processed discs.

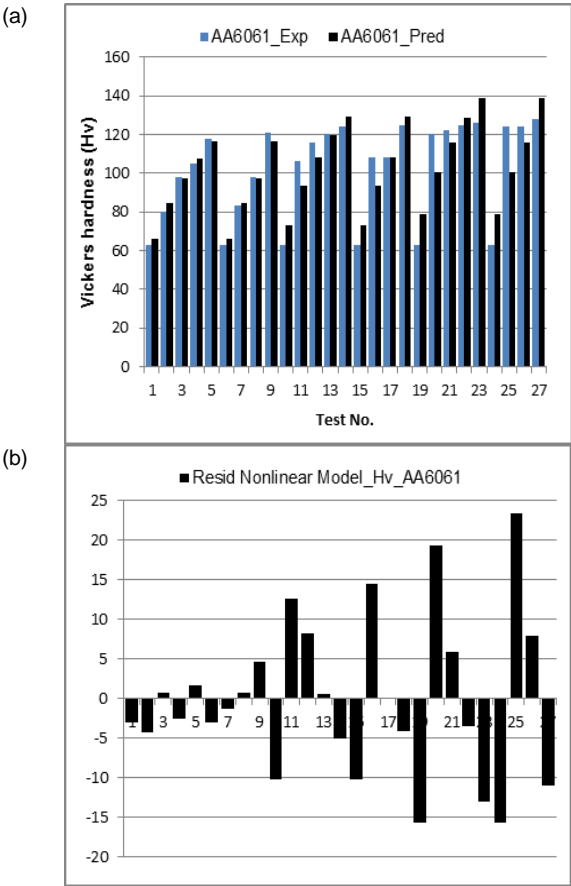


Fig. II. Experimental results vs. predicted data (a) and the residuals distribution (b) of the Hv-values for the HPT processed discs.

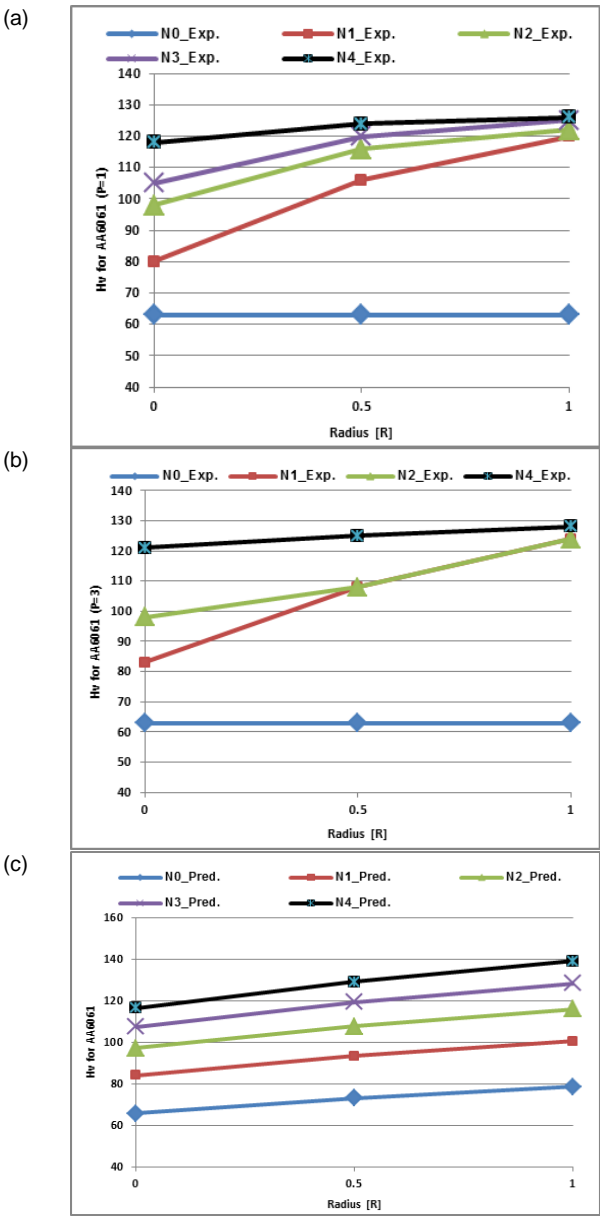


Fig. III. The effect of the position from disc center (R) on Hv-values of AA6061 disc experimentally processed at a pressure of (a) 1 GPa, (b) 3 GPa compared to (c) predicted Hv-values from model (8).

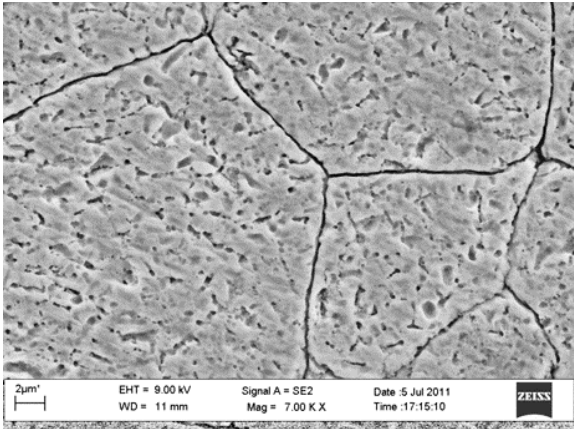


Fig. IV. SEM micrographs of the HCs discs for AA6061.



Fig. V. Experimental results vs. predicted (a, c, and e) and theresiduals distribution (b, d, and f) for (a, b) grains size, (c, d) sub-grains size, and (e, f) substructure size.

Table 1. Experimental date used in the analysis.

Condition		N = 0	N = 1	N = 2	N = 3	N = 4
P = 1GPa	RD %	98.5	99.12	99.2	99.33	99.5
	Hv- at the center (R_0)	63	80	98	105	118
	Hv- at half the radius (0.5R)	63	106	116	120	124
	Hv- at the periphery (R)	63	120	122	125	126
	Yield Stress σ_y (MPa)	220	254	262	279	288
	Compressive Strength σ_c (Mpa)	245	278	289	296	325
	Fracture Strain (ϵ_f %)	30	12	12	10	9
	Grain Size μm	35	33	31	30.4	30
	Subgrain Size μm	3.2	2.8	2.5	2.2	1.9
	Substructure Size	610	360	330	295	250
P = 3GPa	RD %	98.5	99.25	99.3		99.5
	Hv- at the center R_0	63	83	98		121
	Hv- at half the radius 0.5R	63	108	117		125
	Hv- at the periphery R	63	124	124		128
	Yield Stress σ_y (MPa)	220	272	291		312
	Compressive Strength σ_c (Mpa)	245	299	316		339
	Fracture Strain (ϵ_f %)	30	11	9		8
	Grain Size μm	35	32	30.5		30
	Subgrain Size μm	3.2	2	2		1.8
	Substructure Size	610	277	270		240